INTERNATIONAL JOURNAL FOR NUMERICAL METHODS IN FLUIDS, VOL. 24, 101–120 (1997)

AN ADAPTIVE FINITE ELEMENT METHOD FOR A TWO-EQUATION TURBULENCE MODEL IN WALL-BOUNDED FLOWS

F. ILINCA, D. PELLETIER AND A. GARON

CERCA and École Polytechnique de Montréal, PO Box 6079, Succursale Centre-ville, Montréal, Qué. H3C 3A7, Canada

SUMMARY

This paper presents an adaptive finite element method for solving incompressible turbulent flows using a k–ε model of turbulence. Solutions are obtained in primitive variables using a highly accurate quadratic finite element on unstructured grids. A projection error estimator is presented that takes into account the relative importance of the errors in velocity, pressure and turbulence variables. The efficiency and convergence rate of the methodology are evaluated by solving problems with known analytical solutions. The method is then applied to turbulent flow over a backward-facing step and predictions are compared with experimental measurements.

KEY WORDS: incompressible; Navier–Stokes; adaptive FEM; turbulence; k–ε model

1. INTRODUCTION

Adaptive finite element methods provide a powerful approach for tackling complex computational fluid dynamics problems. They can provide accurate solutions at a reasonable cost by automatically clustering elements around flow features of interest such as shear and boundary layers and reattachment points. The adaptive process is also cost-effective in the sense that the best numerical solution is obtained at the least computational cost. Moreover, such approaches provide flexibility in modelling and algorithm development. The ability of the methodology to produce uniformly accurate solutions makes it possible to obtain *numerically exact solutions* (grid-independent) to the equations of motion, so that mathematical models of the physical phenomenon of interest can be evaluated with confidence.

Initial breakthroughs in adaptive computation were achieved in aerodynamics because of the pressing need for accurate computations of shock waves.[1] However, little work has been done for incompressible flows and even less for turbulent flow problems. Proof-of-concept computations for laminar incompressible flow were reported in References 2 and 3. Adaptivity and the $k-\varepsilon$ model are discussed in Reference 4, where structured grids are adapted by both moving nodes and imbedding finer grids in the coarser one. This approach has led to solution improvements. However, the authors performed only one pass of adaption. In this approach the degree of solution improvement is limited by the structured nature of the mesh and the limited number of refinements that are easily implemented (only one step of refinement was implemented). Reference 5 presents applications of an adaptive finite element method to compressible viscous flows with shocks. Turbulence is modelled by a low-Reynolds-number $k-\varepsilon$ model. The adaptive remeshing procedure significantly improved the accuracy of the predictions. However, adaptation was driven by an error estimator that is only sensitive to velocity gradients. In many practical applications the turbulence kinetic energy, its

CCC 0271–2091/97/010101–20

Received 9 December 1994
Revised 4 March 1996

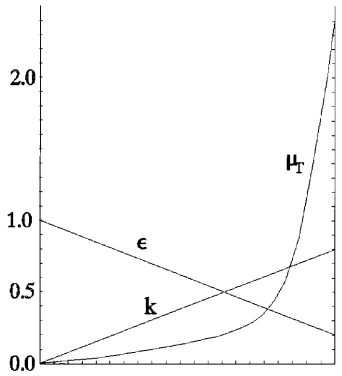

Figure 1. Eddy viscosity variation from linear k and ε

dissipation and the eddy viscosity may have fronts in different locations. Figure 1 illustrates a case where k and ε are linear. They present no front. However, since the eddy viscosity is given by $\mu_T = \rho C_\mu k^2/\varepsilon$, it may present strong variations which are governed by the respective values of the slopes of k and ε.

This paper proposes a practical approach which takes into account the errors in the velocity and turbulence variables and in the eddy viscosity fields. The adaptive strategy is thus sensitive to regions of rapid variations in all dependent variables. This constitutes an improvement over previous work. The use of unstructured grids provides for very high localized grid resolution at a reasonable cost. The remeshing procedure also makes it possible to achieve any preset level of accuracy. The method can thus be viewed as a technique for generating *numerically exact* solutions to the differential equations modeling turbulent flow. In References 6–9 the methodology proposed by the authors was quantitatively validated by solving laminar flows with known analytical solutions and by computing cases for which experimental measurements were available. The methodology was further extended to convective heat transfer flows with variable fluid properties[10] and to zero-equation and two-equation models of turbulence for free shear flows.[11,12] This paper presents a rigorous extension of the methodology to turbulent wall-bounded flows. The methodology is based on adaptive remeshing coupled to a finite element solver for steady state incompressible turbulent flows for which turbulence is represented by the k–ε model.

The paper is organized as follows. First we describe the modelling of the problem. The equations of motion and the finite element solver are reviewed. The turbulence model is discussed and details of the non-linear equation solver and wall boundary conditions are presented. The methodology section describes the error estimator and the adaptive remeshing strategy. The proposed methodology is then validated by solving problems with known analytical solutions to clearly quantify the accuracy improvements due to adaptivity. The method is then applied to turbulent flow over a backward-facing step for which experimental data are available. The paper ends with conclusions.

2. MODELING OF THE PROBLEM

2.1. Reynolds-averaged Navier–Stokes equations

The flow regime of interest is modelled by the Reynolds-averaged Navier–Stokes equations

$$\rho u \cdot \nabla u = -\nabla p + \nabla \cdot [(\mu + \mu_T)(\nabla u + \nabla u^T)] + \rho f, \qquad \nabla \cdot u = 0, \tag{1}$$

where the turbulent viscosity is computed using the $k-\varepsilon$ model of turbulence as

$$\mu_{\mathrm{T}} = \rho C_{\mu} k^2/\varepsilon. \tag{2}$$

The system is closed by including the transport equations for k and ε,[13]

$$\rho u \cdot \nabla k = \nabla \cdot \left[\left(\mu + \frac{\mu_{\mathrm{T}}}{\sigma_k}\right)\nabla k\right] + \mu_{\mathrm{T}} P(u) - \rho\varepsilon, \tag{3}$$

$$\rho u \cdot \nabla \varepsilon = \nabla \cdot \left[\left(\mu + \frac{\mu_{\mathrm{T}}}{\sigma_{\varepsilon}}\right)\nabla \varepsilon\right] + C_1 \frac{\varepsilon}{k}\mu_{\mathrm{T}} P(u) - C_2 \rho \frac{\varepsilon^2}{k}, \tag{4}$$

where the production of turbulence is defined as

$$P(u) = \nabla u : (\nabla u + \nabla u^{\mathrm{T}}). \tag{5}$$

The constants $C_{\mu}, C_1, C_2, \sigma_k$ and σ_{ε} take on the standard values proposed by Launder and Spalding.[13]

To increase the robustness of the finite element scheme, the equations for k and ε are rewritten by using the eddy viscosity definition. Hence, ε may be rewritten as

$$\varepsilon = \rho C_{\mu} k^2/\mu_{\mathrm{T}} \tag{6}$$

to achieve the following block-triangular form of the turbulence equations:

$$\rho u \cdot \nabla k = \nabla \cdot \left[\left(\mu + \frac{\mu_{\mathrm{T}}}{\sigma_k}\right)\nabla k\right] + \mu_{\mathrm{T}} P(u) - \rho^2 C_{\mu} \frac{k^2}{\mu_{\mathrm{T}}}, \tag{7}$$

$$\rho u \cdot \nabla \varepsilon = \nabla \cdot \left[\left(\mu + \frac{\mu_{\mathrm{T}}}{\sigma_{\varepsilon}}\right)\nabla \varepsilon\right] + \rho C_1 C_{\mu} k P(u) - C_2 \rho \frac{\varepsilon^2}{k}. \tag{8}$$

The equations can now be solved in the following order: momentum–continuity, k and then ε.

2.2. Finite element solver

The above equations are solved in a partly segregated manner using the following algorithm:

1. given initial conditions u_0, k_0 and ε_0
2. compute μ_{T} from k and ε
3. for μ_{T} given
   - 3.1. solve momentum and continuity
   - 3.2. solve the k-equation
   - 3.3. solve the ε-equation
   - 3.4. update μ_{T} and go to 3.

In this algorithm, step 3.1 corresponds to solving the Navier–Stokes equations with variable viscosity, for which the proposed adaptive strategy has already proven successful.[10,11] Steps 3.1–3.3 are solved in a Gauss–Seidel fashion, each step using the most recently available values for all variables. Note that in this form of the algorithm the only non-linearities are quadratic ones due to the terms $u \cdot \nabla u, k^2$ and ε^2 which are easily treated with Newton's method.

The finite element equations are obtained by multiplying the differential equations by suitable test functions and applying the divergence theorem to diffusion terms. This leads to the following Galerkin variational equations:

momentum and continuity

$$(\rho u \cdot \nabla u, v) + a(u, v) - (p, \nabla \cdot v) = (f, v) + \langle t^*, v \rangle, \qquad (q, \nabla \cdot u) = 0, \tag{9}$$

with

$$\begin{aligned} (h, g) &= \int_\Omega hg \, \mathrm{d}\Omega, \qquad a(u, v) = \int_\Omega (\mu + \mu_\mathrm{T})(\nabla u + \nabla u^\mathrm{T}) : \nabla v \, \mathrm{d}\Omega, \\ \langle t^*, v \rangle &= \int_{\partial K \setminus \Gamma_\mathrm{t}} [(\mu + \mu_\mathrm{T})(\nabla u + \nabla u^\mathrm{T}) \cdot \hat{n} - p\hat{n}]v \, \mathrm{d}s + \int_{\partial K \cap \Gamma_\mathrm{t}} t^* v \, \mathrm{d}s, \end{aligned} \tag{10}$$

where $\partial K \setminus \Gamma_\mathrm{t}$ denotes either a freestream or outflow boundary and $\partial K \cap \Gamma_\mathrm{t}$ represents the portion of the boundary where the law of the wall will be applied;
turbulence kinetic energy (step 3.2)

$$\int_\Omega \left[\rho u \cdot \nabla k w + \left(\mu + \frac{\mu_\mathrm{T}}{\sigma_k} \right) \nabla k \cdot \nabla w + \rho^2 C_\mu \frac{k^2}{\mu_\mathrm{T}} w \right] \mathrm{d}\Omega = \int_\Omega \mu_\mathrm{T} P(u) w \, \mathrm{d}\Omega; \tag{11}$$

turbulence dissipation (step 3.3)

$$\int_\Omega \left[\rho u \cdot \nabla \varepsilon s + \left(\mu + \frac{\mu_\mathrm{T}}{\sigma_\varepsilon} \right) \nabla \varepsilon \cdot \nabla s + \rho C_2 \frac{\varepsilon^2}{k} s \right] \mathrm{d}\Omega = \int_\Omega \rho C_1 C_\mu k P(u) s \, \mathrm{d}\Omega. \tag{12}$$

These equations are solved in primitive variables using an augmented Lagrangian algorithm to treat the incompressibility.[14] The equations are discretized with the seven-node Crouzeix–Raviart triangular element which uses an enriched quadratic velocity approximation and a linear discontinuous pressure. A standard quadratic interpolant is used for k and ε.

2.3. Wall boundary conditions

On the boundary a combination of Neumann and Dirichlet conditions is imposed by using wall functions which describe the asymptotic behaviour of the different variables near the wall. If the boundary mesh points are located in the logarithmic region, we may impose the wall shear stress given by

$$\tau_\mathrm{w} = \rho u_\tau^2. \tag{13}$$

In equation (10) we then take $t^* = \tau_\mathrm{w} \mathrm{sign}(\bar{u} \cdot \hat{t})\hat{t}$, where $\hat{t}$ is a unit vector tangent to the boundary. The friction velocity u_τ is evaluated by solving the equation

$$Ku = u_\tau \ln\left(E \frac{\rho y}{\mu} u_\tau \right), \tag{14}$$

where u is the tangential velocity, y is the distance to the wall, K is the Karman constant and E is a roughness parameter ($E = 9{\cdot}0$ for smooth walls). Imposing the wall shear stress corresponds to a non-homogeneous Neumann boundary condition for the momentum equation in the tangential direction. The normal component of the velocity is set to zero.

The turbulence kinetic energy (TKE) and its dissipation on the boundary of the mesh are given as functions of the friction velocity:[13]

$$k_\mathrm{w} = u_\tau^2 / \sqrt{C_\mu}, \qquad \varepsilon_\mathrm{w} = u_\tau^3 / Ky. \tag{15}$$

2.4. Stability enhancement measures

The momentum and turbulence transport equations are dominated by convection and it is well known that a standard Galerkin discretization leads to oscillatory solutions. Hence some form of upwinding is required to suppress these unphysical oscillations. Streamline upwinding (SU) as described by Zienkiewicz[15] is used. In this approach the test function for the convective and source terms is modified as

$$W_i = N_i + \frac{\alpha_0}{|V|^2} u_j \frac{\partial N_i}{\partial x_j}, \tag{16}$$

with

$$\alpha_0 = \delta |V| h/2, \tag{17}$$

$$\delta = \coth(Pe) - 1/Pe, \tag{18}$$

where N_i are the interpolation functions, $|V|$ is the speed of the fluid, h is the element size, Pe is the element Peclet number defined as

$$Pe = \rho h |V| / 2k \tag{19}$$

and k is the diffusion coefficient of the transport equation under consideration. This form of upwinding is applied to the momentum and turbulence equations.

The turbulence equations contain divisions by k, ε and μ_T. Hence negative or small values of the denominator can lead to improper sign or overly large values for μ_T or for some source terms. To enhance the robustness of the k–ε algorithm, both k and ε are limited from below to prevent them from taking overly small values. If k is too small, it is replaced by $k = k_{\max}/c_k$, where $k_{\max}$ is the maximum value found in the domain and c_k is a user-supplied constant. If ε is too small and results in overly large values of μ_T, it is replaced by $\varepsilon = \rho C_\mu k^2 / \mathrm{d}_\mu \mu_l$, where d_μ is a user-supplied constant establishing the level of μ_T to $d_\mu \mu_l$. Here μ_l is the fluid viscosity and C_μ is the constant in the k–ε model of Launder and Spalding.[13]

3. ADAPTIVE METHODOLOGY

3.1. Generalities

Most adaptive methods assess the quality of an initial solution obtained on a coarse mesh by using some form of error estimation and modify the structure of the numerical approximation in a systematic fashion to improve the overall quality of the solution. There are several ways of achieving adaptivity: P-methods increase the degree of polynomial approximations for improved accuracy, R-methods relocate grid points in regions of rapid change in the solution[16] and H-methods proceed by either mesh enrichment or remeshing.[1,5]

A variant of an H-method called adaptive remeshing has been retained because it provides the greatest control of element size and grading to accurately resolve flow features such as shear and boundary layers, stagnation points, jets and wakes. In this approach the problem is first solved on a coarse grid to roughly capture the physics of the flow. The resulting solution is then analysed to determine where more grid points are needed and an improved mesh is generated. The problem is solved again on the new mesh using the solution obtained on the coarser mesh as an initial guess. This process is repeated until the required level of accuracy is achieved.

Remeshing also offers an elegant and simple approach to overcome some of the obstacles specific to incompressible viscous flows. For instance, the best proven finite element approximations can be selected based on their convergence and accuracy properties.[14,17] This circumvents the problem associated with P-methods of satisfying the so-called LBB compatibility condition between the velocity and pressure approximations. It also eliminates the 'hanging node problem' encountered in some H-refinement methods.[3]

3.2. Error estimation

This subsection describes the projection error estimation technique used for assessing the accuracy of the solutions obtained by the finite element solver. This error estimator was first introduced by Zienkiewicz and Zhu[18] and involves, in the case of the velocity field, postprocessing of the strain rate tensor $\gamma = (\nabla u + \nabla u^{\mathrm{T}})/2$. The method is based on the observation that while the true derivatives are continuous throughout the flow domain, the finite element derivatives γ_h are discontinuous across element faces. The theory of finite element methods also states that γ_h converges to its true continuous distribution as the mesh is refined. Hence a measure of the quality of the velocity prediction can be obtained by computing the norm of $\gamma_{\mathrm{h}} - \gamma_{\mathrm{ex}}$, where γ_{h} and γ_{ex} are the finite element and exact strain rate respectively.

Unfortunately, the exact solution is not available in practice. However, it has been shown that the exact derivatives can be replaced by a continuous least squares approximation; see References 18 and 19 for details. Thus the velocity error e^u can be estimated by

$$\|e^u\|_{E\Omega} = \left\{ \int_\Omega e^\gamma : e^\gamma \, \mathrm{d}\Omega \right\}^{1/2} = \left\{ \int_\Omega (\tilde{\gamma} - \gamma_{\mathrm{h}}) : (\tilde{\gamma} - \gamma_{\mathrm{h}}) \, \mathrm{d}\Omega \right\}^{1/2}. \tag{20}$$

Here $\tilde{\gamma}$ is a continuous least squares projection of γ_{h} into a space of continuous interpolation functions.

The original global projection method obtains continuous derivatives by solving the least squares problem

$$\min \int_\Omega (\gamma_{\mathrm{h}} - \gamma_{\mathrm{G}})^2 \, \mathrm{d}\Omega, \tag{21}$$

where γ_{h} is the finite element strain rate tensor and γ_{G} is its least squares approximation by the global projection method. Nodal values of γ_{G} are obtained by using the velocity interpolation functions as basis functions for γ_{G}:

$$\gamma_{\mathrm{G}} = \sum \phi_n \{\bar{\gamma}_{\mathrm{G}}\}_n, \tag{22}$$

where ϕ_n are the velocity interpolation functions and $\{\bar{\phi}_{\mathrm{G}}\}_n$ are the nodal values of γ_{G}.

Minimization of the above integral leads to the variational equation

$$\int_\Omega \phi_{\mathrm{m}} (\gamma_{\mathrm{h}} - \gamma_{\mathrm{G}}) \, \mathrm{d}\Omega = 0, \tag{23}$$

which in turn leads to the following symmetric positive definite system of equations for the nodal values $\{\bar{\phi}_{\mathrm{G}}\}_n$:

$$\left[\int_\Omega \phi_{\mathrm{m}} \phi_n \, \mathrm{d}\Omega \right] \{\bar{\gamma}_{\mathrm{G}}\}_n = \int_\Omega \phi_{\mathrm{m}} \gamma_{\mathrm{h}} \, \mathrm{d}\Omega. \tag{24}$$

This approach, originally introduced by Zienkiewicz and Zhu[18] was used with success by the authors in a variety of flow problems.[6–12] However, it was recently shown by Strouboulis and Haque[20] that this approach is not very robust. In same cases the error estimate obtained by computing

$$\|e^u\|^2 = \int_\Omega (\gamma_G - \gamma_h) : (\gamma_G - \gamma_h)\, d\Omega \tag{25}$$

may not be convergent. Examples are given in Reference 20, where this approach yields a value of zero for the error estimate, while the true error given by

$$\|e^u_{ex}\|^2 = \int_\Omega (\gamma_{ex} - \gamma_h) : (\gamma_{ex} - \gamma_h)\, d\Omega \tag{26}$$

is not zero. Reference 20 shows that this improper behaviour persists in spite of mesh refinement. Fortunately, this property occurs on a very specific class of problems: elliptic equations for which the exact solution is a polynomial of degree $k+1$ for a finite element approximation of degree k, where k is even. It is the case for the present finite element solver which uses quadratic interpolations for turbulence variables.

Babuska *et al.*[21] have shown similar trends in more detail for the global projection method. They also show that the local projection technique proposed by Zienkiewicz and Zhu[22,23] leads to a more robust and reliable error estimator. Moreover, the local projection technique leads to correct results when quadratic elements are used to solve the above-mentioned specific cases where the global method failed miserably.

The local projection method[22,23] solves the least squares problem

$$\min \int_{\Omega_s} (\gamma_h - \gamma_L)^2\, d\Omega, \tag{27}$$

where γ_L is the local projection of γ_h. For each node s of the mesh we use the following second-degree polynomial to approximate γ_L:

$$\gamma_L = Pa, \tag{28}$$

where

$$P = [1, x, y, x^2, xy, y^2], \qquad a = [a_1, a_2, a_3, a_4, a_5, a_6]^T. \tag{29}$$

Ω_s is formed by the patch of elements connected to node s. The values of coefficients a_i are obtained by solving the system

$$\left[\int_{\Omega_s} P^T P\, d\Omega\right]\{a\} = \left\{\int_\Omega P^T \gamma_h\, d\Omega\right\}. \tag{30}$$

Then the values of γ_L at nodes are obtained by evaluating

$$\gamma_L(x_s, y_s) = P(x_s, y_s)a. \tag{31}$$

The error in velocity is estimated by

$$\begin{aligned}\|e^u\|^2 &= \int_\Omega (\gamma_L - \gamma_h) : (\gamma_L - \gamma_h)\, d\Omega \\ &= \int_\Omega \left[\left(\frac{\partial u}{\partial x}\right)_L - \left(\frac{\partial u}{\partial x}\right)_h\right]^2 + \frac{1}{2}\left[\left(\frac{\partial u}{\partial y} + \frac{\partial v}{\partial x}\right)_L - \left(\frac{\partial u}{\partial y} + \frac{\partial v}{\partial x}\right)_h\right]^2 + \left[\left(\frac{\partial v}{\partial y}\right)_L - \left(\frac{\partial v}{\partial y}\right)_h\right]^2 \Bigg\} d\Omega,\end{aligned} \tag{32}$$

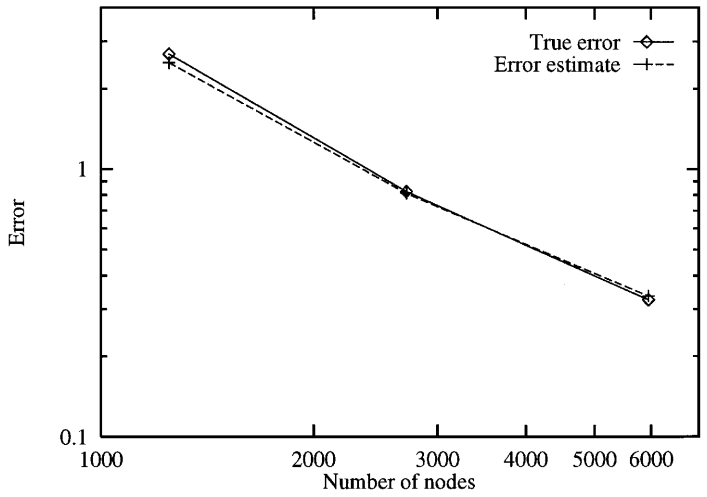

Figure 2. 2D shear layer, trajectory generated by estimator

where the continuous field γ_L is obtained from the nodal values and using the basis of quadratic interpolation functions.

This approach is extended to compute pressure errors:

$$\|e^p\|^2 = \int_\Omega (p_L - p_h)^2 \, d\Omega, \tag{33}$$

where p_L is the continuous least squares fit to p_h, the finite element discontinuous pressure.

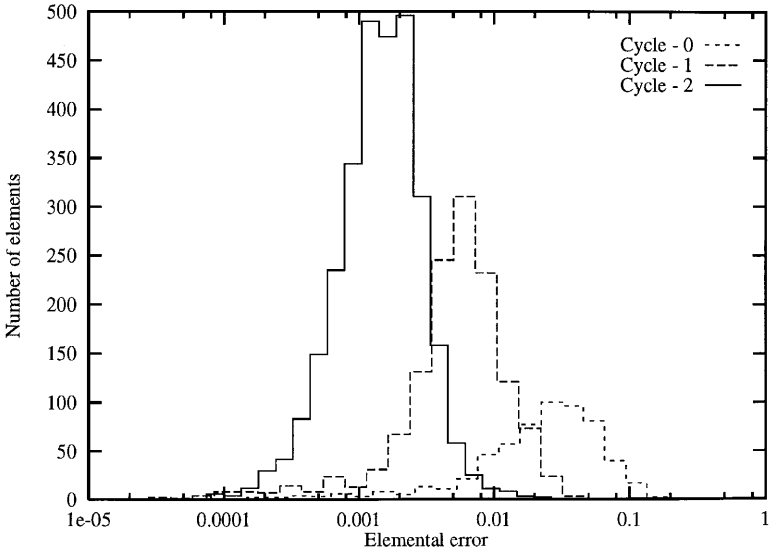

Figure 3. 2D shear layer, histogram of elemental error

Error estimates for turbulence quantities are obtained in a similar fashion:

$$\|e^k\|^2 = \int_\Omega [(\nabla k)_\mathrm{L} - (\nabla k)_\mathrm{h}] \cdot [(\nabla k)_\mathrm{L} - (\nabla k)_\mathrm{h}] \, \mathrm{d}\Omega = \int_\Omega \left\{ \left[\left(\frac{\partial k}{\partial x} \right)_\mathrm{L} - \left(\frac{\partial k}{\partial x} \right)_\mathrm{h} \right]^2 + \left[\left(\frac{\partial k}{\partial y} \right)_\mathrm{L} - \left(\frac{\partial k}{\partial y} \right)_\mathrm{h} \right]^2 \right\} \mathrm{d}\Omega, \tag{34}$$

$$\|e^\varepsilon\|^2 = \int_\Omega [(\nabla \varepsilon)_\mathrm{L} - (\nabla \varepsilon)_\mathrm{h}] \cdot [(\nabla \varepsilon)_\mathrm{L} - (\nabla \varepsilon)_\mathrm{h}] \, \mathrm{d}\Omega = \int_\Omega \left\{ \left[\left(\frac{\partial \varepsilon}{\partial x} \right)_\mathrm{L} - \left(\frac{\partial \varepsilon}{\partial x} \right)_\mathrm{h} \right]^2 + \left[\left(\frac{\partial \varepsilon}{\partial y} \right)_\mathrm{L} - \left(\frac{\partial \varepsilon}{\partial y} \right)_\mathrm{h} \right]^2 \right\} \mathrm{d}\Omega. \tag{35}$$

An error estimator is also constructed for the eddy viscosity, since slowly varying k and ε can result in an eddy viscosity presenting rapid variations or fronts. The error estimator is defined as

$$\begin{aligned} \|e^{\mu_\mathrm{T}}\|^2 &= \int_\Omega [(\nabla \mu_\mathrm{T})_\mathrm{L} - (\nabla \mu_\mathrm{T})_\mathrm{h}] \cdot [(\nabla \mu_\mathrm{T}) - (\nabla \mu_\mathrm{T})_\mathrm{h}] \, \mathrm{d}\Omega \\ &= \int_\Omega \left\{ \left[\left(\frac{\partial \mu_\mathrm{T}}{\partial x} \right)_\mathrm{L} - \left(\frac{\partial \mu_\mathrm{T}}{\partial x} \right)_\mathrm{h} \right]^2 + \left[\left(\frac{\partial \mu_\mathrm{T}}{\partial y} \right)_\mathrm{L} - \left(\frac{\partial \mu_\mathrm{T}}{\partial y} \right)_\mathrm{h} \right]^2 \right\} \mathrm{d}\Omega. \end{aligned} \tag{36}$$

It should be noted that k, ε and μ_T generally take values that are several orders of magnitude smaller than the velocity. Hence their error estimates will be much smaller than those on u. However, both k and ε directly after u through their ratio $\mu_\mathrm{T} = \rho C_\mu k^2/\varepsilon$. Hence an accurate solution for both k and ε is required to obtain a meaningful velocity field. To ensure that turbulence errors are of the same order as the velocity errors, the velocity and turbulence fields are scaled to their maximum values. The total error is then computed as

$$\|(e^u, e^p, e^k, e^\varepsilon, e^{\mu_\mathrm{T}})\| = \left(\frac{\|e^u\|^2}{u_\mathrm{max}^2} + \frac{\|e^p\|^2}{p_\mathrm{max}^2} + \frac{\|e^k\|^2}{k_\mathrm{max}^2} + \frac{\|e^\varepsilon\|^2}{\varepsilon_\mathrm{max}^2} + \frac{\|e^{\mu_\mathrm{T}}\|^2}{\mu_{\mathrm{T}_\mathrm{max}}^2} \right)^{1/2}. \tag{37}$$

3.3. Adaptive remeshing

There remains to discuss how one exploits the knowledge of the error distribution to design a better mesh. The adaptive remeshing strategy is straightforward and follows that proposed in Reference 1, proceeding as follows:

1. generate an initial mesh
2. compute the finite element solution
3. compute error estimate
4. if (global error $\leqslant$ tolerance) then
   - stop

   else
   - compute grid density from error estimate
   - generate an improved mesh according to grid density
   - interpolate current solution on new mesh

   go to 2

   end if.

We now provide details on some of the steps of this algorithm. Once the finite element solution has been obtained, the error on each element is computed using one of the previously described

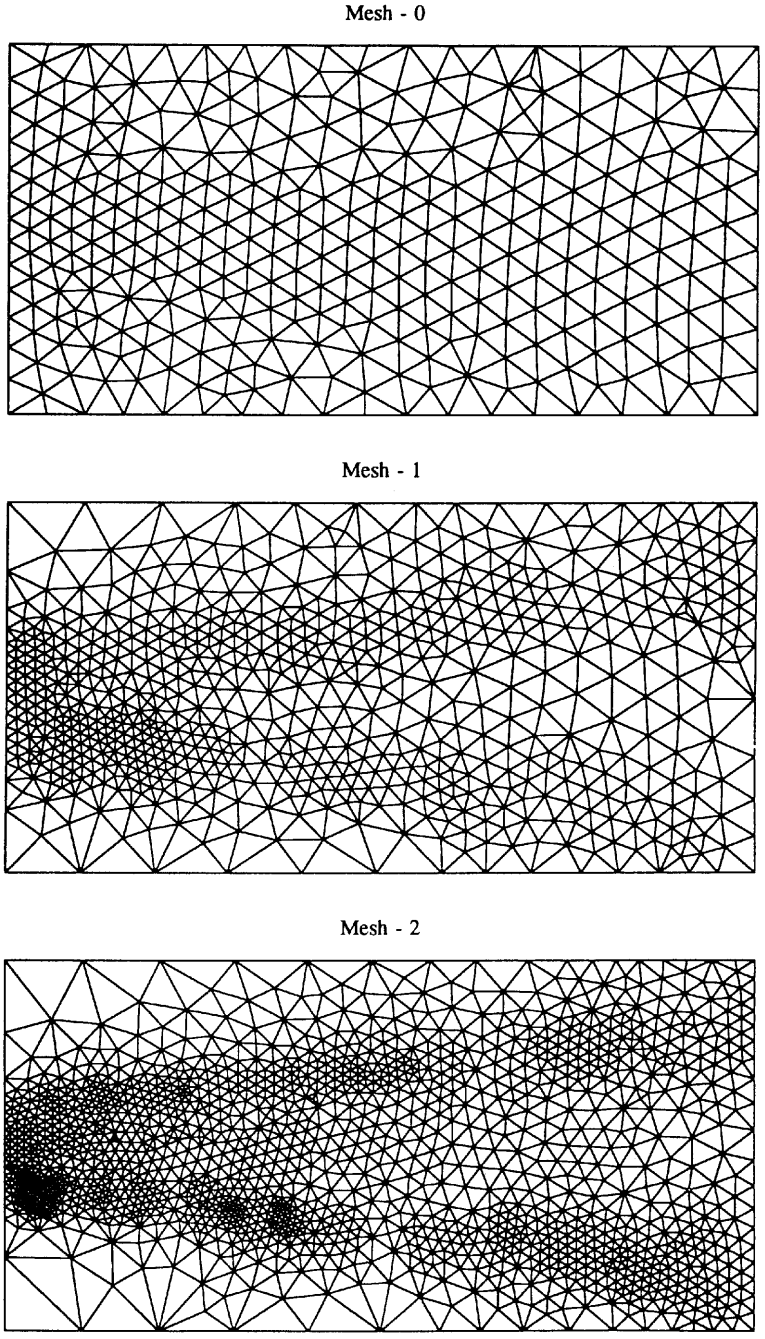

Figure 4. 2D shear layer, meshes generated by adaptive procedure

Table I. 2D shear layer

Mesh	Number of nodes	Number of elements	Solution norm	Error estimate	True error
0	1247	594	5·578	2·492	2·684
1	2709	1326	5·442	8·120e-1	8·254e-1
2	5953	2940	5·454	3·361e-1	3·252e-1

estimators. The global norms of the solution and the error are computed as

$$\|e_{\text{tot}}\|^2 = \sum \|e_k\|^2. \tag{38}$$

There remains to compute the element size for the improved mesh so that elements are smaller in regions of large error and bigger in regions where the solution is already accurate. This is achieved by requiring that the improved mesh be optimal (i.e that all elements have the same average error $\mathbf{e}_{\text{av}}$). Now, given a target reduction coefficient of the error, ξ, the total and average errors can be related

$$\|e_{\text{av}}\| = \xi \|e_{\text{tot}}\| / \sqrt{n}. \tag{39}$$

Finally, an expression for element sizes can be derived from the asymptotic rate of convergence of the finite element approximation which relates the error on each element to some power k ($k = 2$ for the present case) of the element size h:

$$\|e\| = ch^k, \tag{40}$$

which can also be written for the target elemental error as

$$\|e_{\text{av}}\| = c\delta^k. \tag{41}$$

These two equations can be solved for the required element size:

$$\delta = \left(\frac{\xi \|e_{\text{tot}}\|}{\|e\| \sqrt{n}} \right)^{1/k} h. \tag{42}$$

This distribution of element size is then used as the grid function in an advancing front mesh generator[1] in order to generate an improved mesh.

4. VALIDATION

The error estimators are first compared on a simple flow problem for which an analytical solution is known. This provides controlled conditions for validating the methodology and assessing its computational performance.

Convergence was achieved when the relative error on two successive global iterates was less than 10^{-6}. In all cases, subiterations on u, k and ε were performed until the relative error and the L_2 norms of residuals were of the order of 10^{-8}. The adaptive procedure and finite element code were run in a blackbox fashion with no intervention on the part of the user. The adaptive procedure was set to reduce the global error by a factor of three at each cycle of adaptation.

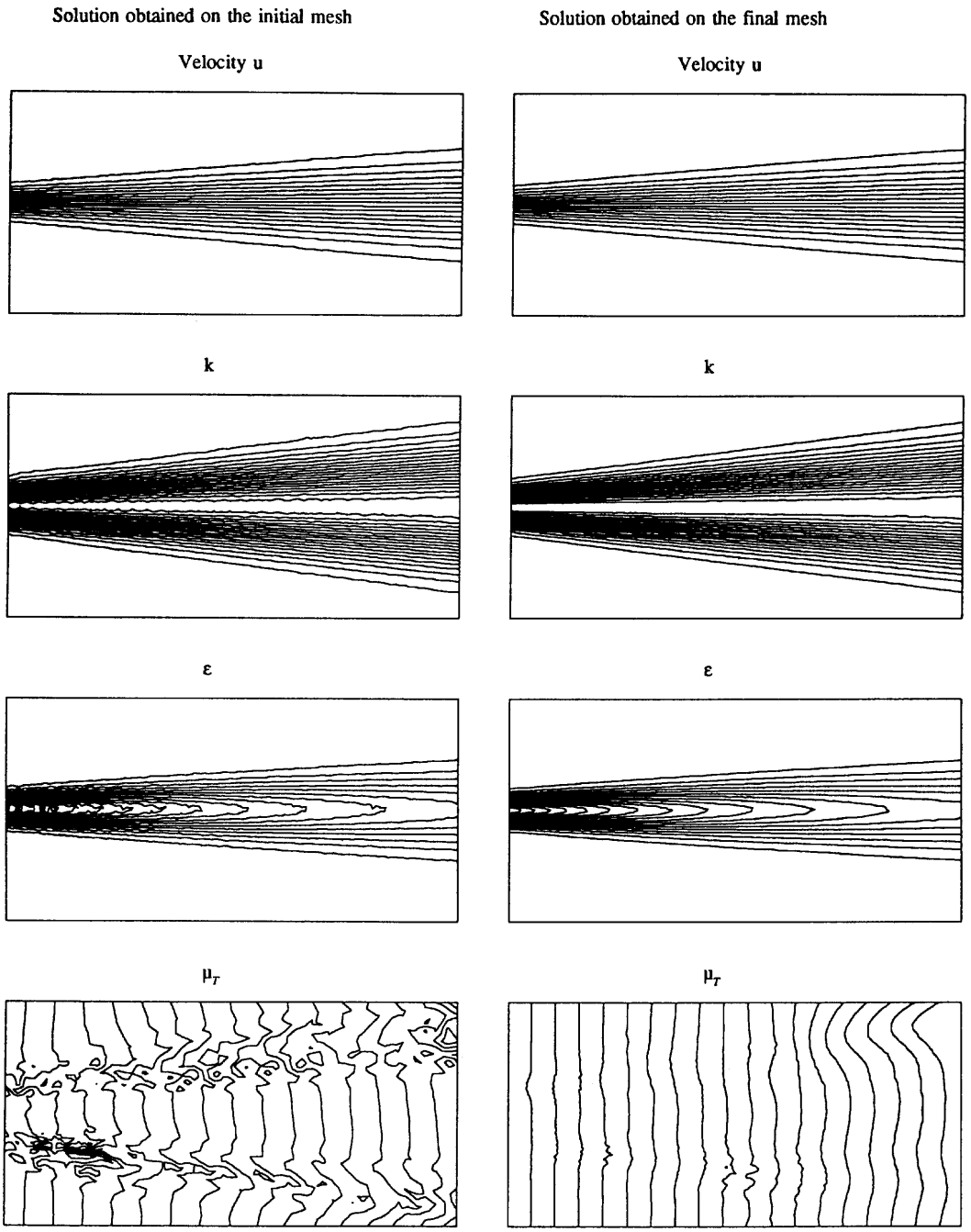

Figure 5. Solutions on initial and final meshes

4.1. A 2D shear layer with linear turbulent viscosity

This is a version of the shear layer described by Schlichting[24] consisting of two coflowing streams of velocities u_1 and u_2. The solution is assumed to be

$$u = \frac{u_1 + u_2}{2} - \frac{u_1 - u_2}{2}\operatorname{erf}\left(\frac{\sigma y}{x}\right), \qquad v = \frac{u_1 - u_2}{2}\frac{1}{\sigma\sqrt{\pi}}\exp\left[-\left(\frac{\sigma y}{x}\right)^2\right],$$
$$p = 0, \qquad k = k_0\left\{c_k + \exp\left[-\left(\frac{\delta y}{x}\right)^2\right]\right\}, \qquad \varepsilon = \frac{\varepsilon_0}{x}\left\{c_k + \exp\left[-\left(\frac{\sigma y}{x}\right)^2\right]\right\}^2, \qquad \mu_T = \mu_{T_0} x. \tag{43}$$

The constants are taken to be

$$u_1 = 1{\cdot}0, \qquad u_2 = 0{\cdot}0, \qquad \sigma = 13{\cdot}5,$$
$$k_0 = \frac{343}{75000}u_1(u_1 - u_2)\frac{\sigma}{\sqrt{\pi}}, \qquad \varepsilon_0 = \frac{343}{22500}C_\mu u_1(u_1 - u_2)^2\frac{\sigma^2}{\pi}, \tag{44}$$
$$\mu_{T_0} = \frac{343}{250000}\rho u_1, \qquad Re_1 = \frac{\rho u_1 L}{\mu_1} = 10^4.$$

Table I presents the performance of the projection estimator. As can be seen, both the true error and its estimate decrease at each cycle of adaptation. The error levels obtained are comparable for the true and estimate errors, indicating that the projection error estimator performs adequately. Figure 2 illustrates the trajectory generated by the estimator. As can be seen, the behaviour of the estimator follows closely that of the true error.

Figure 3 is a histogram of the elemental error. It is a count of the elements having the same level of error. In an ideal situation all elements would have the same error. In practice we obtain an approximately Gaussian distribution. As can be seen from this figure, the error is reduced throughout the domain at each cycle of adaptation. Furthermore, the proportion of the elements clustered near the mean increases from one cycle to another, indicating that the meshes tend towards optimality.

Figure 4 illustrates meshes generated by the procedure. As can be seen, the adaptation strategy proceeds by a complete reallocation of grid points, refining the mesh around the fronts of k and near the centre of the shear layer in the mid-section of the domain. Contour lines of the velocity, turbulence kinetic energy, turbulence dissipation and turbulence viscosity are presented in Figure 5. The plots on the left represent the solution obtained on the initial coarse mesh, while those on the right present the solution on the final mesh. As can be seen, the resolution improves drastically between the initial and the final mesh. Predictions obtained after adaptation show very good resolution for the turbulence variables, especially for the turbulent viscosity, which must vary only in the x-direction.

Finally, Figure 6 compared contour lines of the velocity, turbulence kinetic energy, dissipation and turbulent viscosity errors and of the combined error evaluated on the second mesh. The plots on the left are contours of the true errors; those on the right are contours of the error estimate. One can see that the key features of the errors in the shear layer are reproduced by the estimator. This indicates that the error estimator is faithful to the true error. This constitutes a significant improvement over our previous results.[12]

In summary, the adaptive procedure performs well and leads to solution improvements.

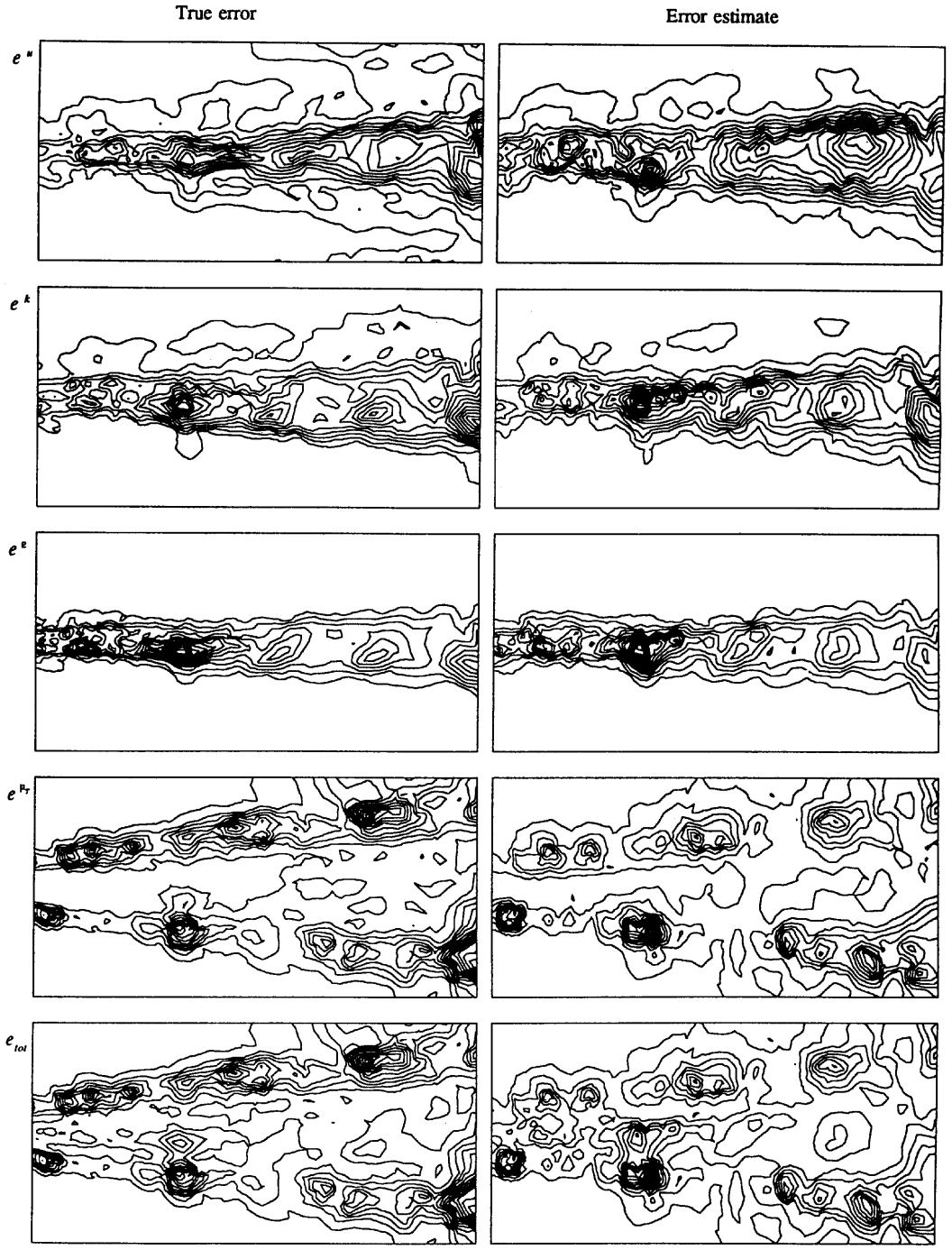

Figure 6. Contour lines of velocity, turbulence kinetic energy, dissipation and turbulent viscosity errors and of combined error

5. APPLICATION: FLOW OVER A BACKWARD-FACING STEP

This problem has been the subject of a detailed experimental study by Kim[25] and has served as a benchmark for turbulent flow solvers. Typical meshes generated by the adaptive strategy are shown in Figure 7. As can be seen, the mesh is highly refined near the corner of the step, in the shear layer and in the boundary layer on the bottom wall. The solution obtained on the final mesh is shown in Figure 8. As can be seen, k and μ_T present steep fronts in the shear layer and along the bottom wall, while ε presents a peak next to the corner.

Figure 9 presents a comparison of predicted and measured streamwise velocity profiles at selected stations. As can be seen, the agreement is good for all stations and improves with adaptivity. Table II summarizes the results obtained for the length of the recirculation zone.

These results should be viewed as excellent in view of the large scatter of predicted values reported by Nallasamy.[26]

Figure 10 presents a comparison of predicted and measured turbulence kinetic energy. It should be noted that Kim[25] provides values of $\bar{u}^2$ and $\bar{v}^2$ only. Hence it is impossible to assess the exact values of k in the experiment. Consequently, at each station the TKE is scaled by its maximum value as reported by most authors. The agreement is good. The adaptive strategy has captured the very thin layer and peak in the TKE profile at $x/HT = 1{\cdot}0$. The steep front at $x/HT = 2{\cdot}3$ is also very nicely resolved, although measurements indicate a lower slope of the TKE profile.

Figure 11 shows distribution of the main components of the Reynolds stress tensor at selected stations. As observed by Nallasamy,[26] the $k-\varepsilon$ model predicts higher values of $\overline{uv}$ than measured in the initial region of the shear layer and lower values than measured downstream of the reattachment point. As can be seen, the predictions are qualitative in nature but are as accurate as the best published results[27,28] obtained on a mesh of more than 48,000 points. The present predictions required less than 7000 nodes.

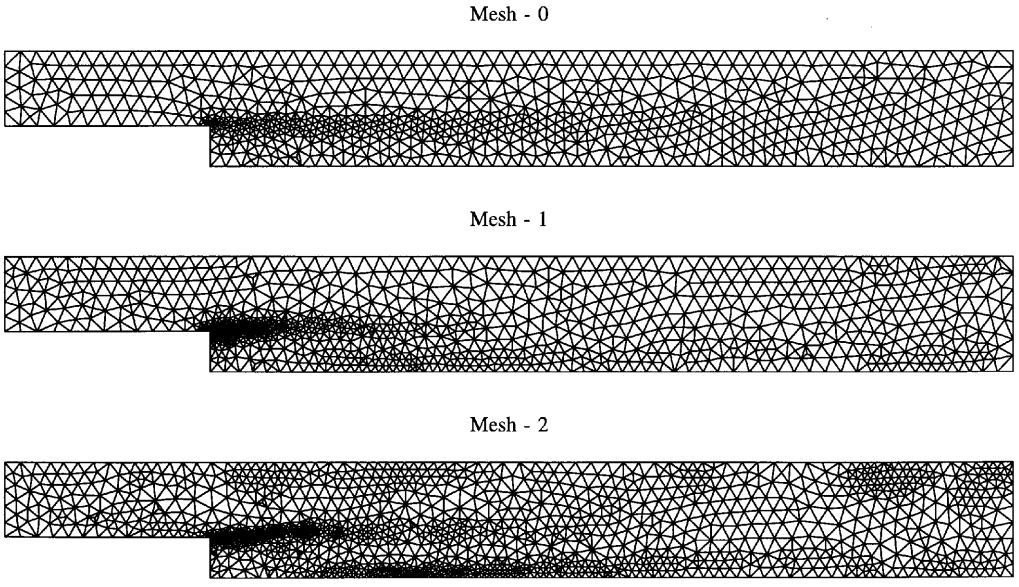

Figure 7. Meshes generated by adaptive procedure

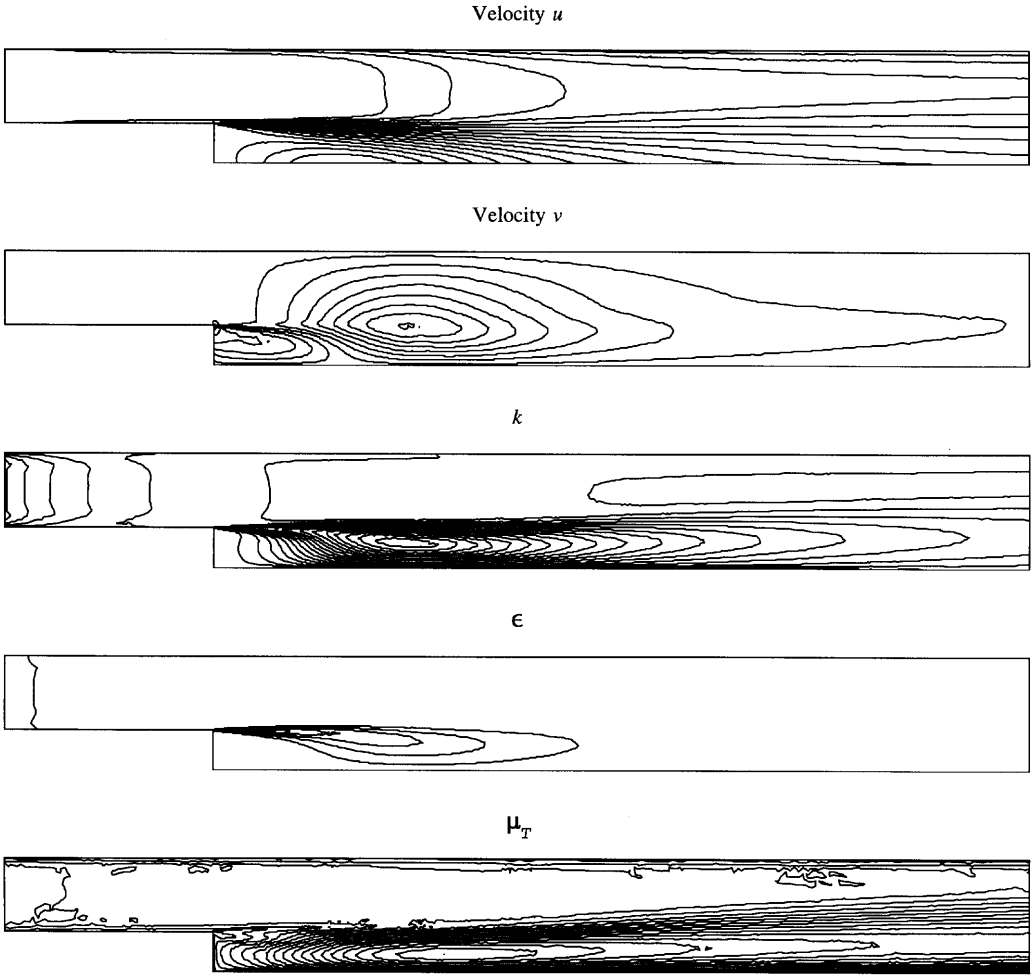

Figure 8. Solution obtained on final mesh

Table II. Length of recirculation zone

Code/experiment	Length	Error (%)
Experiment	7·00	—
Mesh 0 (3123 points)	5·630	20
Mesh 1 (4690 points)	6·022	14
Mesh 2 (6960 points)	6·206	11
Reference 23 (48,472 points)	5·588	20
Reference 24 (10,458 points)	5·5	21

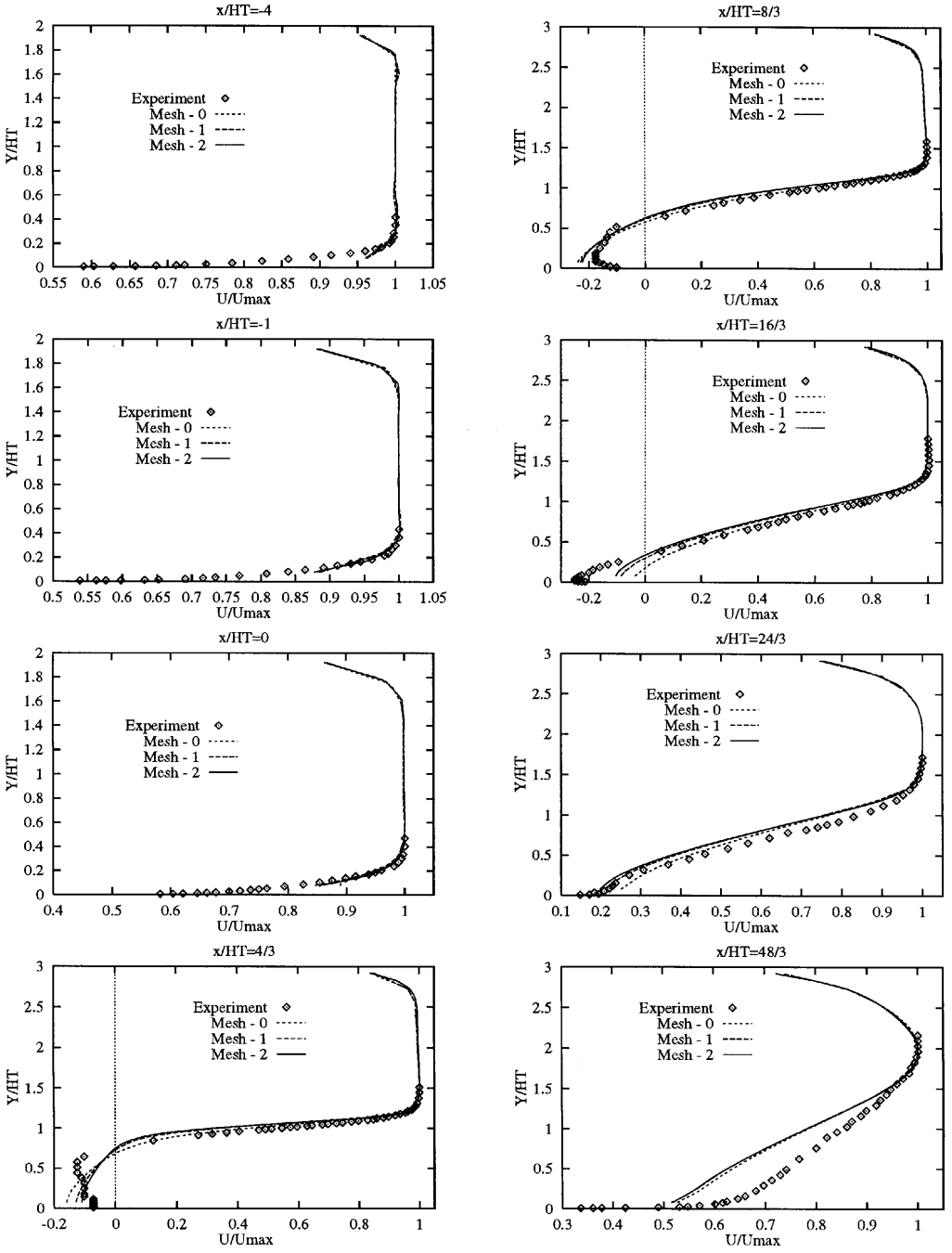

Figure 9. Measured and predicted streamwise velocity profiles

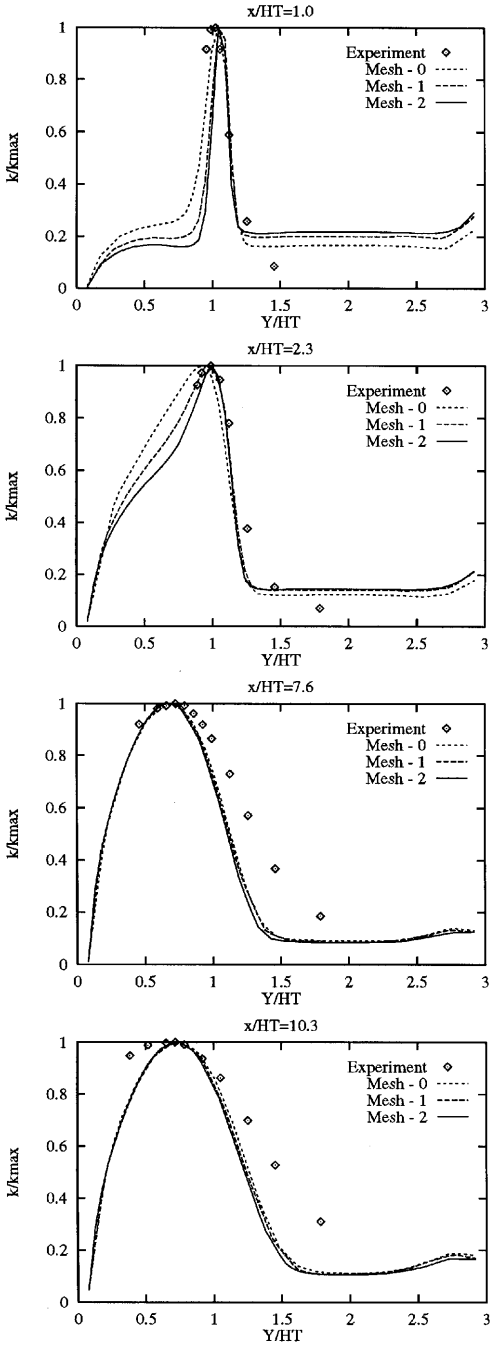

Figure 10. Distribution of turbulence kinetic energy

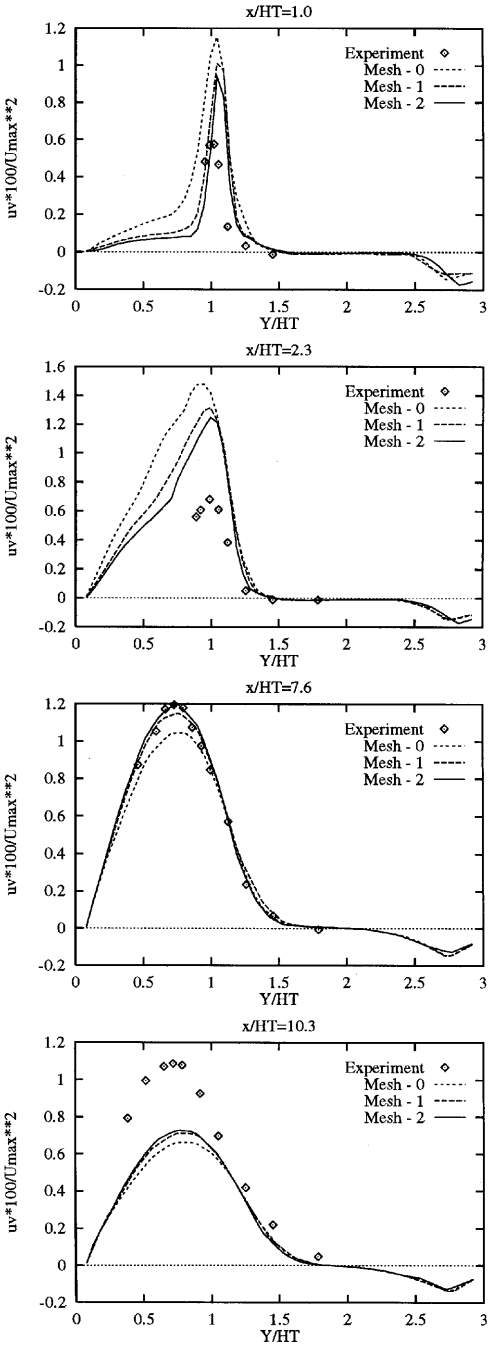

Figure 11. Distribution of Reynolds stress tensor

6. CONCLUSIONS

An adaptive remeshing strategy has been presented for the $k-\varepsilon$ model of turbulence based on a projection technique for computing an error estimator. The estimator incorporates errors from all sources: velocity, pressure and turbulence variables and eddy viscosity fields. The adaptive strategy have proven reliable and convergent on non-trivial problems with analytical solutions.

For internal flow over a backward-facing step the technique leads to very good predictions. The velocity field and length of the recirculation zone are well predicted. The predictions of the TKE are less accurate and more sensitive to changes in the mesh. Finally, the predictions of the Reynolds stress are even more mesh-sensitive but are in qualitative agreement with measurements. They are at least as accurate as the best published results.

ACKNOWLEDGEMENT

This work was supported by Direction des Études at Recherche d'Électricité de France with Drs. J.-P. Chabard and G. Pot as technical monitors.

REFERENCES

1. J. Peraire, M. Vahdati, K. Morgan and O. C. Zienkiewicz, 'Adaptive remeshing for compressible flows', *J. Comput. Phys.*, **72**, 26–37 (1987).
2. J. Wu, J. Z. Zhu, J. Szmelter and O. C. Zienkiewicz, 'Error estimation and adaptivity in Navier–Stokes incompressible flows', *Comput. Mech.*, **6**, 259–270 (1990).
3. K. C. Wang and G. F. Cary, 'Adaptive grids for coupled viscous flow and transport', *Comput. Methods Appl. Mech. Eng.*, **82**, 365–383 (1990).
4. F. Moukalled and S. Acharya, 'Application of an adaptive grid procedure for the calculation of turbulent separated flows', *Comput. Fluids*, **21**, 455–473 (1992).
5. G. R. Vemeganti and R. K. Prabhu, 'Application of a two-equation turbulence model for high speed compressible flows using unstructured grids', *AIAA Paper 93-3029*, 1993.
6. J. F. Hétu, D. Pelletier, 'Adaptive remeshing for viscous incompressible flows', *AIAA J.*, **30**, 1986–1992 (1992).
7. J. F. Hétu and D. Pelletier, 'A fast adaptive finite element scheme for viscous incompressible flows', *AIAA J.*, **30**, 2677–2682 (1992).
8. D. Pelletier and J.-F. Hétu, 'An adaptive finite element methodology for incompressible viscous flows', in *Advances in Finite Element Method in Fluid Dynamics*, FED Vol. 137, ASME, New York, 1992, pp. 1–12.
9. D. Pelletier, J.-F. Hétu and F. Ilinca, 'Adaptive finite element method for thermal flow problems', *AIAA J.*, **32**, 741–747 (1994).
10. D. Pelletier, F. Ilinca and J.-F. Hétu, 'An adaptive finite element method for convective heat transfer with variable fluid properties', *J. Thermophys. Heat Transfer*, **8**, 687–694 (1994).
11. D. Pelletier, F. Ilinca and J.-F. Hétu, 'An adaptive finite element method for turbulent free shear flow past a propeller', *AIAA Paper 93-3388*, 1993.
12. D. Pelletier and F. Ilinca, 'Adaptive remeshing for the $k-\varepsilon$ model of turbulence', *AIAA Paper 94-0818*, 1994.
13. B. E. Launder and J. Spalding, 'The numerical computation of turbulent flows', *Comput. Methods Appl. Mech. Eng.*, **3**, 269–289 (1974).
14. D. Pelletier and A. Fortin, 'Are FEM solutions of incompressible flows really incompressible? (or how simple flows can cause headaches)', *Int. j. numer. methods fluids*, **9**, 99–112 (1989).
15. O. C. Zienkiewicz, *The Finite Element Method*, 3rd edn, McGraw-Hill, New York, 19XX.
16. R. Lohner, K. Morgan and O. C. Zienkiewicz, 'Adaptive grid refinement for the Euler and compressible Navier–Stokes equations', in *Accuracy Estimates and Adaptive Refinement in Finite Element Computations*, Wiley, New York, 1986.
17. M. Fortin and A. Fortin, 'Experiments with several elements for incompressible flows', *Int. j. numer. methods fluids*, **5**, 911–928 (1985).
18. O. C. Ziekiewicz and R. J. Z. Zhu, 'A simple error estimator and adaptive procedure for practical engineering analysis', *Int. j. numer. methods eng.*, **24**, 337–357 (1987).
19. J. F. Hétu, 'Méthodes d'éléments finis adaptives pour les écoulements visquex incompressibles', *Ph.D. Thesis, École Polytechnique de Montréal, 1991*.
20. T. Strouboulis and K. A. Haque, 'Recent experience with error estimation and adaptivity, part I: Review of error estimators for scalar elliptic problems', *Comput. Method Appl. Mech. Eng.*, **97**, 399–436 (1992).

21. I. Babuska, T. Strouboulis and C. S. Upadhyag, 'A model study of the quality of a posteriori error estimators for linear elliptic problems. Error estimation in the interior of pathwise uniform grids of triangles', *Comput. Methods Appl. Mech. Eng.*, **114**, 307–378 (1994).
22. O. C. Zienkiewicz and J. Z. Zhu, 'The superconvergent patch recovery and a posteriori error estimates. Part 1: The recovery technique', *Int. j. numer. methods eng.*, **33**, 1331–1364 (1992).
23. O. C. Zienkiewicz and J. Z. Zhu, 'The superconvergent patch recovery and a posteriori error estimates. Part 2: Error estimates and adaptivity', *Int. j. numer. methods eng.*, **33**, 1365–1382 (1992).
24. H. Schlichting, *Boundary Layer Theory*, 7th edn, McGraw-Hill, New York, 1979, pp. 737–739.
25. J. J. Kim, 'Investigation of separation and reattachment of turbulence shear layer: flow over a backward facing step', *Ph.D. Thesis*, Stanford University, 1978.
26. M. Nallasamy, 'Turbulence models and their applications to the prediction of internal flows: a review', *Comput. Fluids*, **15**, 151–194 (1987).
27. S. Thangham and N. Hur, 'A highly resolved numerical study of turbulent separated flow past a backward facing step', *Int. J. Eng. Sci.*, **29**, 607–615 (1991).
28. C. G. Speziale and N. Tuan, 'Numerical solution of turbulent flow past a backward facing step under a non-linear $k-\varepsilon$ model', *Int. J. Eng. Sci.*, **26**, 1099–1112 (1988).